

## *Retraction*

# **Retracted: Application and Value of Dynamic Volume CT Multiparameter Imaging in the Diagnosis of Traumatic High-Flow Penile Abnormal Erection**

### **Scientific Programming**

Received 17 October 2023; Accepted 17 October 2023; Published 18 October 2023

Copyright © 2023 Scientific Programming. This is an open access article distributed under the Creative Commons Attribution License, which permits unrestricted use, distribution, and reproduction in any medium, provided the original work is properly cited.

This article has been retracted by Hindawi following an investigation undertaken by the publisher [1]. This investigation has uncovered evidence of one or more of the following indicators of systematic manipulation of the publication process:

- (1) Discrepancies in scope
- (2) Discrepancies in the description of the research reported
- (3) Discrepancies between the availability of data and the research described
- (4) Inappropriate citations
- (5) Incoherent, meaningless and/or irrelevant content included in the article
- (6) Peer-review manipulation

The presence of these indicators undermines our confidence in the integrity of the article's content and we cannot, therefore, vouch for its reliability. Please note that this notice is intended solely to alert readers that the content of this article is unreliable. We have not investigated whether authors were aware of or involved in the systematic manipulation of the publication process.

Wiley and Hindawi regrets that the usual quality checks did not identify these issues before publication and have since put additional measures in place to safeguard research integrity.

We wish to credit our own Research Integrity and Research Publishing teams and anonymous and named external researchers and research integrity experts for contributing to this investigation.

The corresponding author, as the representative of all authors, has been given the opportunity to register their agreement or disagreement to this retraction. We have kept a record of any response received.

### **References**

- [1] C. Xu, X. Ruan, Y. Pan, and Q. Huang, "Application and Value of Dynamic Volume CT Multiparameter Imaging in the Diagnosis of Traumatic High-Flow Penile Abnormal Erection," *Scientific Programming*, vol. 2021, Article ID 4234177, 7 pages, 2021.

## Research Article

# Application and Value of Dynamic Volume CT Multiparameter Imaging in the Diagnosis of Traumatic High-Flow Penile Abnormal Erection

Chengcheng Xu , Xinzhong Ruan , Yuning Pan , and Qiuli Huang 

Department of Radiology, Ningbo First Hospital, Ningbo City 315010, Zhejiang Province, China

Correspondence should be addressed to Xinzhong Ruan; 2015211125@smail.jsut.edu.cn

Received 19 June 2021; Accepted 8 September 2021; Published 25 September 2021

Academic Editor: Arunkumar N

Copyright © 2021 Chengcheng Xu et al. This is an open access article distributed under the Creative Commons Attribution License, which permits unrestricted use, distribution, and reproduction in any medium, provided the original work is properly cited.

**Objective.** To explore the clinical application of dynamic volume CT multiparameter imaging in the observation of penile hemodynamics in patients with abnormal vascular erections. **Methods.** 90 patients with suspected vascular abnormal erections treated in our hospital from January 2016 to January 2020 were included in the study, and 40 patients with psychologically abnormal erections were selected for the control. The corpus cavernosum injection vasoactive drug test (ICI) and dynamic volume CT and Doppler ultrasound were used to test the hemodynamics of the corpus cavernosum of all selected patients and to analyze the changes of penile length, circumference, systolic peak flow rate, diastolic peak flow rate, and blood flow resistance index in different types of penile erection disorder patients before and after ICI test. **Results.** Among the 90 patients with suspected vascular abnormal erection, 34 patients had arterial abnormal erection, 25 patients had venous abnormal erection, and 31 patients had mixed vascular abnormal erection. In patients with arterial abnormal erection and mixed vascular abnormal erection, penile cavernous body diameter, PSV, and abnormal erection  $V$  are smaller than those in patients with venous abnormal erection and psychological abnormal erection, while arterial abnormal erection and psychological abnormal erection are obviously higher in RI than venous abnormal erection and mixed vascular abnormal erection, and the difference is statistically significant ( $P < 0.05$ ). Before the ICI test, there was no significant difference in the penis circumference and length between the four groups of patients with arterial abnormal erection, venous abnormal erection, mixed vascular abnormal erection, and psychological abnormal erection ( $P > 0.05$ ); after the ICI test, patients with arterial abnormal erections had significantly shorter penis perimeter and penis length than those with venous abnormal erections, mixed vascular abnormal erections, and psychological abnormal erections ( $P < 0.05$ ). **Conclusion.** Dynamic volume CT can clearly reflect the penile hemodynamic state of patients with vascular abnormal erections, provide a powerful diagnostic basis for accurately and effectively determining the classification of vascular abnormal erections, and be worthy of popularization and clinical use.

## 1. Introduction

Abnormal erection usually means that the penis cannot continue to achieve or maintain enough erection to obtain a satisfactory sex life. Its main pathological basis is due to the hemodynamic changes in the cavernous body of the penis. Abnormal erections mainly include vascular abnormal erections, psychological abnormal erections, and mixed abnormal erections. How to distinguish them accurately is very important for the clinical treatment of abnormal erection. In this study, 90 patients with suspected vascular

abnormal erections were subjected to penile corpus cavernosum injection vasoactive drug test (ICI), and dynamic volume CT and Doppler ultrasound were used to detect and diagnose hemodynamics of the corpus cavernosum. The specific reports are as follows [1].

## 2. Materials and Methods

**2.1. Clinical Data.** Randomly selected 90 patients with suspected vascular abnormal erections treated in our hospital from January 2016 to January 2020 were included

in this study. All patients included in the study were married. After the study was approved and reviewed by the ethics committee of our hospital, all patients began to sign the informed consent form. At the same time, 40 patients with abnormal psychological erections were selected as controls. Before dynamic volume CT multiparameter imaging examination, all patients received luteinizing hormone, serum testosterone, and other examinations, and all examination indicators were at normal levels, excluding patients with abnormal development of sexual organs. The baseline conditions of the two groups are shown in Table 1.

## 2.2. Method

**2.2.1. Equipment.** The instrument used was Aquilion ONE 320 CT (Toshiba Corporation, Japan).

**2.2.2. Operation Method.** The patient was guided to lay a supine position. The internal iliac artery to the penis was scanned. 50–80 mL nonionic contrast medium was injected through the elbow vein at a rate of 4.5–5 mL/s. 320 dynamic volume CT scanning was used, with the slice thickness of 0.5 mm. Single scanning rotation was 0.75 s at 80 kV. Generally, the image slice thickness was kept at about 0.5 mm. Each volume data could hold 320 CT images. Each examination could produce more than 3,200 images. Afterward, all the data were imported by the 4D-DSA software package of Toshiba to generate 4D dynamic vascular images. Then, images were processed by multiple planar reconstruction (MPR), maximum intensity projection (MIP), and volume rendering (VR) to display the lesion site more clearly. The diagnosis of the standard internal pudendal artery, internal penile artery, and penile dorsal artery was partly interrupted. The contrast agent in some images overflowed, and pseudoaneurysm formed in some images. Therefore, traumatic priapism was considered. ICI test was performed on the patients, and 1 mg of vasoactive drug (30 mg papaverine hydrochloride + 10 mg/mL phentolamine) was injected into the cavernous body. After 5 minutes, massage was used to induce penile erection, and its length and circumference were measured. Then, the Doppler ultrasound was used to detect bilateral deep penile arteries, peak systolic velocity (PSV), peak end-diastolic velocity, and blood flow resistance index (RI) [2, 3].

**2.3. Other Clinical Data.** Erectile hardness: the erectile hardness of low-flow priapism is grade 4 (complete erection, hardness is hard), the skin temperature is low, the color is dark purple, the pain is obvious, and the arterial pulse is rarely touched. The erectile hardness of high-flow PP is grade 2-3 (incomplete erection, general hardness), skin temperature is slightly higher, arterial pulsation is palpable, and mild pain is observed.

Urine routine examination: hematuria, indicating injury, positive correlation.

Blood gas analysis: blood was drawn from the cavernous body of the penis. Blood of low-flow priapism was dark purple. The result of blood gas analysis of the corpus cavernosum was hypoxic hypercapnia. If  $PO_2 < 30$  mmHg,  $pCO_2 > 60$  mmHg, and  $pH < 7.25$ , it could be considered as ischemic priapism. The blood gas analysis of high-flow priapism was similar to that of arterial blood, and the results showed that it was normal; the blood gas analysis results of some high-flow priapism with severe injury were similar to those of low-flow priapism.

**2.4. Principle of Dynamic Volume Multiparameter CT Imaging.** The ray source  $S$  makes a circular motion with the radius  $D$  as the center of the coordinate origin  $O$ , and the detector line ( $t$ -axis) also rotates around the coordinate origin  $O$ . The position of the ray source is represented by the angle  $\theta$  between the central ray  $SO$  and the  $x$ -axis, and the detector line is perpendicular to the straight line where the central ray is located, as shown in Figure 1.

Let  $\vec{r} = [x, y]^T$  indicate the position of a point in the image and  $\tau(\theta, \vec{r})$  the position where the ray intersects the  $t$ -axis after passing through the point (see  $\tau(\theta, \vec{r})$  in Figure 1). At the angle  $\theta$  and detector  $t$ , the fan-beam projection of the detected object  $f(Pf)(\theta, t)$  is obtained by linear interpolation of the parameter  $(\theta, t)$ . If it is a complete scan,  $\theta_{\max} = 2\pi$ ; if it is a short scan or an overscan,  $\theta_{\max}$  may be other values. First, the fan-beam projections are weighted and ramp-filtered to generate the fan-beam projection  $g(p, t)$  corresponding to the source angle  $\theta_p$ . Then, the image is reconstructed by the following traditional FBP reconstruction algorithm:

$$f(\vec{r}) = \sum_{p=0}^{P-1} W(p\Delta\theta, \vec{r})g[p, \tau(p\Delta\theta, \vec{r})]\Delta\theta. \quad (1)$$

Among them,  $W(\theta, \vec{r})$  is the corresponding weighting function. In the image reconstruction process, after the introduction of FFT, the calculation amount of weighting and ramp filtering is only  $O(N^2 \lg N)$ , but the back-projection requires  $O(N^3)$  calculation amount, so the key to speeding up the reconstruction process is to improve the backprojection algorithm [4].

The idea of the fast-FBP algorithm comes from the parallel-beam fast segmentation backprojection reconstruction algorithm (FHBP), and its final total reconstruction calculation amount is reduced to  $O(N^2 \lg N)$ . Dalal and Erlich [5] described the parallel-beam FHBP in detail.

In the fast-FBP algorithm, we construct the same segmentation algorithm to directly handle the fan-beam projection. We use the same layered structure to reconstruct 1/4 images from half the number of fan-beam projections. However, because the fan-beam projection after the image is moved is different from the fan-beam projection after moving the original image, it is necessary to modify the moving object in order to continue to use the hierarchical structure in the fan-beam CT [5].

Consider the backprojection operation of  $f$ 's subimage  $f'(\vec{r})$  (see Figure 1). Let  $KM(\vec{\delta})$  be an image interception

TABLE 1: Baseline data of two groups of patients.

Project	Suspected vascular abnormal erection	Abnormal psychological erection	$t/\chi^2$	$P$
Age	$34.6 \pm 5.4$	$35.8 \pm 6.2$	1.758	0.080
Smoking history (cases)	36	16	2.232	0.135
History of alcoholism (example)	23	14	0.310	0.578
Luteinizing hormone ( $\mu\text{g/L}$ )	$14.2 \pm 1.7$	$14.1 \pm 1.6$	0.497	0.6198
Serum testosterone (nmol/L)	$15.6 \pm 1.1$	$15.8 \pm 1.0$	1.550	0.1221
Complicated disease (case)				
Hypertension	11	6	0.635	0.4255
Diabetes	9	5	0.299	0.5844
Hypertension	12	2	0.473	0.4914

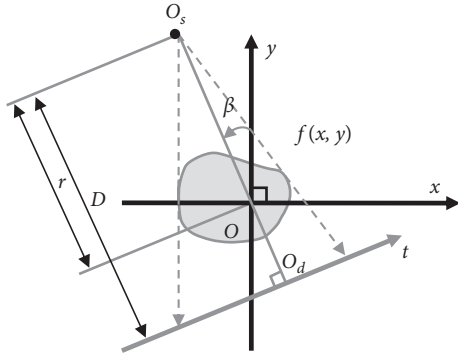


FIGURE 1: Schematic diagram of fan-beam CT scanning.

expression so that  $f' = KM(\vec{\delta})f$  is an  $M \times M$  subimage with the center at  $O'$ . Using  $Q$  projections, at  $p\Delta\theta, p=0, \dots, Q-1$ , the backprojection of the subimage  $f'$  is directly derived by formula (1):

$$f'(r) = B_{M,Q}(\vec{\delta})g(\vec{r}), \quad (2)$$

where  $B_{M,Q}(\vec{\delta})$  is the corresponding backprojection expression. If  $f = B_{N,P}(\vec{0})g$  is available,

$$\begin{aligned} f' &= K_M(\vec{\delta}), \\ f &= B_{M,P}(\vec{\delta})K_M(\vec{\delta})g. \end{aligned} \quad (3)$$

This shows that the backprojection of  $f'$  can be obtained by the corresponding backprojection (size is  $(M, P)$ ). Consider that image  $f$  is divided into 4  $(N/2) \times (N/2)$  subimages that do not overlap each other:

$$f = \sum_{j=1}^4 K_{N/2}(\vec{\delta}_j)f. \quad (4)$$

Here,  $\vec{\delta}_j, j=1, 2, 3, 4$ , is the center of each subimage. Substituting into formula (2), the accurate segmentation formula of the original image backprojection can be obtained:

$$\begin{aligned} f &= B_{N,P}[\vec{0}]g \\ &= \sum_{j=1}^4 B_{N/2}[\vec{\delta}_j]K_{N/2}[\vec{\delta}_j]g. \end{aligned} \quad (5)$$

Compared with single-step backprojection  $B_{N,P}$ , the above segmentation will not speed up the backprojection

process. In fact, the calculation amount of backprojection  $B_{M,P}$  of a single subimage is 4 times less than the  $c(N/2)^2 p$  calculation amount of single step  $B_{N,P}$  of the entire image, but the total calculation of the backprojection of four subimages is not much smaller than that of single step  $B_{N,P}$ .

The fast-FBP algorithm mainly reduces the amount of calculation by reconstructing a subimage  $f' = K_M \vec{\delta} f$  from a smaller number of projections ( $P/L$ ). The process of reducing the number of projections is as follows: on the  $t$ -axis, the intercepted projection  $K_M \vec{\delta} g(\theta p, t)$  of  $f'$  is moved by  $\tau(\theta, \vec{\delta})$  (see Figure 1), thereby reducing the  $P$  projections to  $P/L$ , and then the  $\tau(\theta, \vec{\delta})$  projection can be moved by  $D$ . Move back to the original position. Using  $O(L, M, \vec{\delta})$  to describe the projection reduction operation, backprojection formula (2) of the subimage  $f'$  can be written as

$$\begin{aligned} f' &= K_{M,P} \vec{\delta} f \\ &= B_{M,P/L} \vec{\delta} g' \\ &= B_{M,P/L} \vec{\delta} O(L, M, \vec{\delta})g. \end{aligned} \quad (6)$$

Among them,  $B_{M,P/L}$  is the backprojection of  $M \times M$  subimages when using  $P/L$  projections. This can derive the approximate segmentation of the original image backprojection:

$$\begin{aligned} f' &= B_{N,P} \vec{0} g' \\ &= \sum_{j=1}^4 B_{N/2,P/2} \vec{\delta} O(2, N/2, \vec{\delta})g. \end{aligned} \quad (7)$$

According to the iterative division equation (7), the subgraph obtained by the previous division can be further divided. This iterative process can be performed continuously until the subimage reaches the desired size  $M_{\min}$ , and then backprojection  $B_{P_{\min}}, M_{\min}$  is performed. Optimal  $M_{\min}$  is usually determined by the actual operation. It can be selected as small as possible, such as  $M_{\min} = 1$ , so that the size of the smallest subimage is 1 pixel. At this point, there is an  $\lg^2 N$ -step decomposition. The final step will include  $N^2$  single-pixel backprojections  $B_{P,N,1}$  with a computational cost of  $cPN$ . When performing  $O(PN \lg N)$ , assuming that fixed-length interpolation is used to reduce and shift the projection operation, it can be shown that the calculation amount for each segmentation will be  $c_1 NP$ . Therefore, the total computational cost of the  $\lg^2 N$  step is  $O(N^2 \lg N)$ .

Since  $P = O(N)$ , the total computational volume of the iterative segmentation algorithm is  $O(N^2 \lg N)$ , and the computational volume of the backprojection process is  $O(N^2 \lg N)$ .

**2.5. Statistical Analysis.** All the data involved in this study were statistically analyzed using SPSS 18.0 software. The measurement data were expressed in the form of mean  $\pm$  standard deviation. For data comparison, the measurement data used the  $t$ -test, while the count data were tested using the chi-square test for comparison, and the difference was statistically significant when  $P < 0.05$ .

### 3. Results

**3.1. Dynamic Volume CT Multiparameter Imaging Display Results and the Distribution of Vascular Abnormal Erections.** After 320 CT volume scan in the cavernous arterial phase, the image processing showed a spindle-shaped columnar, smooth, and symmetrical high-density shadow on both sides of the corpus cavernosum and a strip of low-density shadow in the middle of the cavernous body on both sides corresponding to the cavernous interval. Under normal circumstances, the urethra cavernous body and the penis head were not developed. Before the ICI test, the dynamic volume CT can clearly show the penile corpus cavernosum, tunica albuginea, and urethra. When weak, the cavernous artery diameter is small, and the intermittent blood flow signal can be seen during the systole; after the ICI test, the corpus cavernosum increases sharply. Judging by the results of dynamic volume CT examination, among the patients with suspected vascular abnormal erections, 34 cases (37.78%) had arterial abnormal erections, 25 cases (27.78%) had venous abnormal erections, and 31 cases (34.44%) had mixed vascular abnormal erections. The 320 CT volume scan of various types of deep penile arteries is shown in Figures 2 and 3.

**3.2. Hemodynamics of Patients with Different Types of Abnormal Erections.** Comparing the hemodynamic parameters of patients with different types of abnormal erections, it is found that the diameter of the cavernous body, PSV, and abnormal erection  $V$  of patients with arterial abnormal erection and mixed vascular abnormal erection are less than those of patients with venous abnormal erection and psychological abnormal erection. They have statistical significance ( $P < 0.05$ ); arterial abnormal erection and psychological abnormal erection are significantly higher in RI than venous abnormal erection and mixed vascular abnormal erection, and the difference is statistically significant ( $P < 0.05$ ) (Table 2).

**3.3. Changes in Penile Girth and Length of Patients with Different Types of Abnormal Erection before and after ICI.** Before the ICI test, there were no significant differences in penile girth and length between the four groups of patients with arterial abnormal erection, venous abnormal erection, mixed vascular abnormal erection, and psychological

abnormal erection ( $P > 0.05$ ); after the ICI test, in patients with arterial abnormal erections, the penis perimeter and penis length were significantly shorter than those in patients with venous abnormal erections, mixed vascular abnormal erections, and psychological abnormal erections ( $P < 0.05$ ). See Table 3.

### 4. Discussion

The normal erection of the penis is the result of the coordinated action of human psychology, endocrine, nerves, and hemodynamics. Abnormal erection usually refers to that the penis cannot continue to achieve or maintain enough erection to obtain a satisfactory sexual life. Its main pathological basis is due to changes in hemodynamics in the corpus cavernosum. There are several clinically abnormal erections: organic abnormal erection, psychological abnormal erection, and mixed abnormal erection. Among them, organic abnormal erection accounts for about 60% to 90%. The etiology is mainly vascular, including arterial abnormal erection about 20% to 30% and mixed vascular abnormal erections accounting for about 40% to 50%. No matter what kind of abnormal erection is related to the abnormal hemodynamics of the cavernous body of the penis, observation of the hemodynamic state of the cavernous body of the penis is of great significance for the differential diagnosis of vascular abnormal erections. As a noninvasive and painless inspection method that can be continuously and dynamically observed and repeated, dynamic volume CT has a significant effect on evaluating penile hemodynamics and can play a positive role in the clinical diagnosis, classification, and location of the abnormal erection.

The erectile process of the penis can be divided into three stages, vascular stage, fascia stage, and white membrane stage, which is the result of a series of neurovascular activities. The degree of erection is closely related to the balance of the arterial blood inflow and venous blood outflow of the cavernous body of the penis. Therefore, the perfect coordination between the arterial blood supply, vein closure, and reflux system is the key to maintaining the full erection of the penis. During this period, changes in hemodynamics of the cavernous body of the penis are particularly important. Among the three stages of penile erection, the vascular stage is the active stage, and the other two stages are the passive stage. In the vascular stage, after the penile arteries are dilated, a large amount of arterial blood flow enters the cavernous body of the penis and expands it. At this time, the penis outflow veins are blocked, but the erectile function of the penis is normal. Once the vascular stage is blocked, the following two stages cannot be completed. Whether the vascular stage is blocked can often be judged by PSV, abnormal erection  $V$ , RI, and other indicators. According to relevant research, under the condition that the penile venous occlusion system is complete, the lack of blood supply to the cavernous artery of the penis will definitely lead to the decrease of PSV. Therefore, PSV is the main parameter for judging the abnormal erection of the cavernous artery. Abnormal erection  $V$  and RI are important indicators for judging venous abnormal erection. RI is a

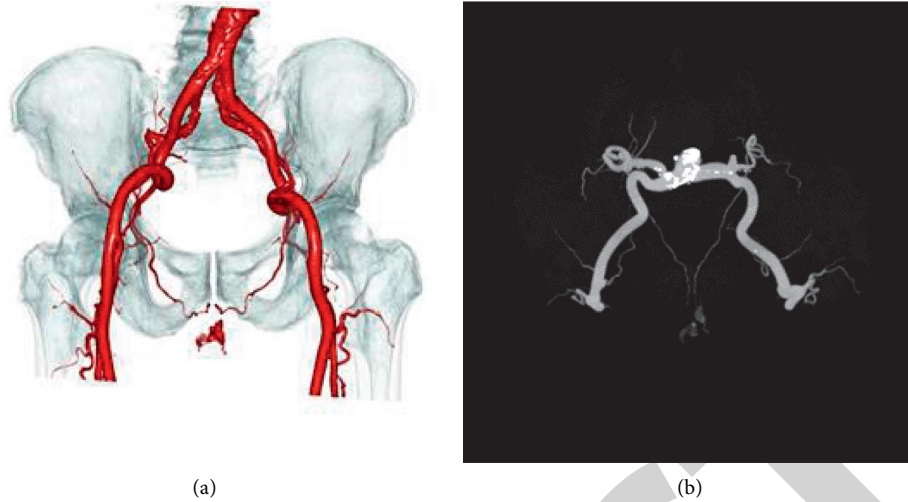


FIGURE 2: Bilateral internal penile artery injury with bilateral pseudoaneurysm formation: (a) virtual reality, transparency, and overlap technology are added; (b) maximum intensity projection (MIP).

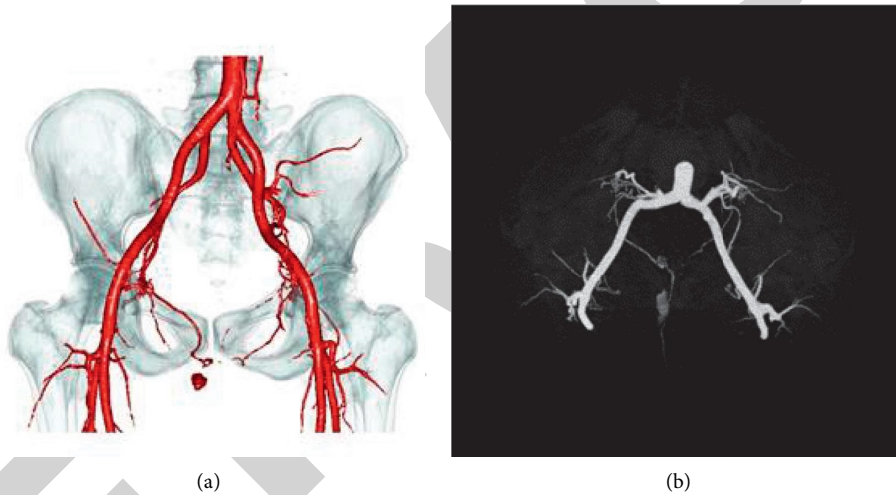


FIGURE 3: Right dorsal penile artery injury with pseudoaneurysm and left pudendal artery injury: (a) virtual reality, transparency, and overlap technology are added; (b) maximum intensity projection (MIP).

TABLE 2: Comparison of hemodynamic parameters of patients with different types of abnormal erection.

Types	Number of cases	Inner diameter (mm)	PSV (cm/s)	Abnormal erection V (cm/s)	RI
Arterial abnormal erection	34	0.83 ± 0.12 <sup>a</sup>	19.4 ± 3.1 <sup>a</sup>	1.2 ± 0.4 <sup>a</sup>	1.0 ± 0.2
Venous abnormal erection	25	0.92 ± 0.15	42.8 ± 5.1	5.6 ± 1.4	0.6 ± 0.1 <sup>b</sup>
Mixed vascular abnormal erection	31	0.86 ± 0.12 <sup>a</sup>	33.2 ± 4.2 <sup>a</sup>	5.2 ± 1.1 <sup>a</sup>	0.7 ± 0.1 <sup>b</sup>
Abnormal psychological erection	40	0.93 ± 0.16	47.3 ± 5.5	0.2 ± 0.1	1.1 ± 0.2

Compared with venous abnormal erection and psychological abnormal erection, <sup>a</sup> $P < 0.05$ ; compared with arterial abnormal erection and psychological abnormal erection, <sup>b</sup> $P < 0.05$ .

reflection of the resistance of the corpus cavernosum artery blood flow and is closely related to the pressure around the blood vessel, the strength of the penis, and the internal pressure. If there is abnormal erection  $V > 5$  cm/s and  $RI < 1$ , there may be venous leakage [6].

The location of abnormal erectile vascular lesions caused by trauma varies according to age and etiology. In older

patients, with increasing age, cardiovascular disease gradually appears, vascular disease of abnormal penile erection is a part of systemic vascular system disease, and the position is relatively high, while young patients have large life and work activities and are susceptible to obvious or undetected perineal injury, which causes relatively low vascular lesions in the penis. Rosen et al. performed selective internal pudendal



TABLE 3: Comparison of penile girth and length of patients with different types of abnormal erection before and after ICI treatment.

Types	Number of cases	Before ICI		After ICI	
		Penis circumference (mm)	Penis length (mm)	Penis circumference (mm)	Penis length (mm)
Arterial abnormal erection	34	75.4 ± 11.4	63.6 ± 8.1	89.4 ± 12.8 <sup>a</sup>	98.3 ± 10.9 <sup>a</sup>
Venous abnormal erection	25	76.1 ± 12.1	63.2 ± 8.3	96.8 ± 14.1	105.7 ± 12.4
Mixed vascular abnormal erection	31	75.7 ± 11.6	64.1 ± 7.9	99.7 ± 13.9	109.0 ± 11.8
Abnormal psychological erection	40	75.5 ± 11.9	64.2 ± 8.5	103.1 ± 14.5	114.2 ± 12.8

Compared with venous abnormal erection, mixed vascular abnormal erection, and psychological abnormal erection, <sup>a</sup> $P < 0.05$ .

arteriography in 195 patients with abnormal penile erection caused by trauma at an average age of 35.4. Most patients had lesions in the cavernous artery of the penis, while in another group of older patients, the lesions were mainly located in the internal iliac artery and internal pudendal artery. Leveine et al. conducted a corresponding study on patients with erectile dysfunction after blunt injury of the pelvis or vulva. The lesions in patients with blunt pelvic erectile dysfunction may be the internal pudendal artery, cavernous artery, and dorsal penile artery, among which the distal end of the internal pudendal artery had the highest lesion rate (92%).

In this study, the PSV of the arterial abnormal erection group was only  $19.4 \pm 3.1$  cm/s, which was significantly lower than the normal level, and the abnormal erection  $V$  and RI were in the normal range, so it was clearly diagnosed as arterial abnormal erection; the abnormal erection  $V$  of the venous abnormal erection group was  $5.6 \pm 1.4$  cm/s, and the RI was  $0.6 \pm 0.1$ . There was basically venous leakage, which could be diagnosed as venous abnormal erection, while the mixed abnormal erection group PSV is obviously low, abnormal erection  $V > 5$  cm/s,  $RI < 1$ , and it has the clinical characteristics of arterial abnormal erection and venous abnormal erection and can be diagnosed as mixed abnormal erection.

This result also proves that the hemodynamics of the cavernous body of the penis is an important criterion for the diagnosis of vascular abnormal erection and vein type, and it is also one of the main factors that leads to abnormal erection of patients. In addition, in this study, there were significant differences in penis length and perimeter between patients with different types of abnormal erection before and after ICI-induced penile erection. Among them, psychological abnormal erection had the largest length and perimeter after erection. Because patients with abnormal psychological erections are only due to psychological effects, the length and circumference of the penis after the drug-induced erection are relatively normal. However, patients with arterial abnormal erection, venous abnormal erection, and mixed vascular abnormal erection have a certain degree of lesions due to their own blood supply, vein closure, and reflux system, so the blood supply is not full after the erection. There is something missing. According to the average value of penile erection length and perimeter of abnormal erection patients under normal circumstances, it can basically determine whether the cause of the patient's morbidity is caused by psychological effects [7].

In this study, six patients with erectile dysfunction were enrolled, including three patients with lesions located in the distal internal pudendal artery and three patients with lesions located in the cavernosal artery. Due to the small number of cases, it is difficult to make further comparative analysis. However, compared with selective arteriography, dynamic volume CT penile artery imaging can display the location of abnormal erection of the arterial penis; its three-dimensional stereoscopic image can also be observed with multiangle and multiaxis rotation, which can make the diseased blood vessels. The site is displayed more clearly and intuitively; in addition, it can remove the influence of the pelvis, etc., which is also impossible for selective arteriography. Of course, the use of dynamic volume CT penile artery imaging for the diagnosis of arterial penile abnormal erection is still in its infancy, but it has shown its unique advantages; through the continuous accumulation and analysis of the number of cases, I believe that this imaging technology will become selective, an alternative method of arteriography, or a screening method for the abnormal erection of the arterial penis. Selective pudendal angiography is still the main method for assessing the location and characterization of penile blood supply abnormalities [8].

## 5. Conclusion

In summary, dynamic volume CT is the main screening method for the differential diagnosis of abnormal erections. In the differential diagnosis of vascular abnormal erections, it can accurately judge arterial, venous, and mixed abnormal erections. It is worthy of extensive application in clinical diagnosis.

## Data Availability

The data used to support the findings of this study are available from the corresponding author upon request.

## Conflicts of Interest

The authors declare no conflicts of interest.

## Acknowledgments

This work was supported by the Medical and Health Science and Technology Program of Zhejiang Province (no. 2018KY152).

## References

- [1] L. Dell'Atti, "The role of ultrasonography in the diagnosis and management of penile trauma," *Journal of Ultrasound*, vol. 19, no. 3, pp. 161–166, 2016.
- [2] S. Mori, R. Hirai, and Y. Sakata, "Using a deep neural network for four-dimensional CT artifact reduction in image-guided radiotherapy," *Physica Medica*, vol. 65, pp. 67–75, 2019.
- [3] R. Multescu, R. Satalan, D. Georgescu, and P. Geavlete, "P-05-017 penile trauma: apropos of two cases," *The Journal of Sexual Medicine*, vol. 13, no. 5, p. 223, 2016.
- [4] S. Wu, M. Wang, and Y. Zou, "Research on internet information mining based on agent algorithm," *Future Generation Computer Systems*, vol. 86, pp. 598–602, 2018.
- [5] A. Dalal and Y. Erlich, "Mondor'," *Journal of the Royal Army Medical Corps*, vol. 162, no. 1, pp. 66-67, 2016.
- [6] R. Multescu, M. Stan, V. Iordache et al., "512 penile trauma secondary to aggression—particularities and prognosis," *The Journal of Sexual Medicine*, vol. 15, no. 7, pp. 311-312, 2018.
- [7] Q. Ke, S. Wu, M. Wang, and Y. Zou, "Evaluation of developer efficiency based on improved DEA model," *Wireless Personal Communications*, vol. 102, no. 4, pp. 3843–3849, 2018.
- [8] M. Falcone, G. Garaffa, A. Raheem, N. A. Christopher, and D. J. Ralph, "Total phallic reconstruction using the radial artery based forearm free flap after traumatic penile amputation," *The Journal of Sexual Medicine*, vol. 13, no. 7, pp. 1119–1124, 2016.